Korean J. Chem. Eng., 40(9), 2199-2208 (2023)
DOI: 10.1007/s11814-023-1470-7

pISSN: 0256-1115
eISSN: 1975-7220

Surface modification of petroleum residue-activated carbon using citric acid for enhanced cobalt removal from an aqueous solution

Jong-Soo Choi*, Choong Jeon, and Suk Soon Choi*,†**

*Department of Biological and Environmental Engineering, Semyung University, Jecheon 27136, Korea
**Department of Biochemical Engineering, Gangneung-Wonju National University, Gangneung 25457, Korea
(*Received 12 March 2023 • Revised 5 April 2023 • Accepted 10 April 2023*)

Abstract−Although the amount of petroleum residues produced from oil refinery processes has increased, there has been limited research for the residues. In this work, we developed petroleum residue-activated carbon (PAC) by chemical modification with citric acid as a novel adsorbent The optimal concentration of citric acid for PAC was chosen as the 6 M (named PAC-CA6) and the adsorption behavior of Co(II) was investigated. The experimental data were analyzed using various isotherm and kinetic models. The maximum adsorption capacity of 12.50 mg/g was determined using the Langmuir model. The pseudo-second-order model was found to be the most suitable for describing the adsorption kinetics. PAC-CA6 was characterized by using various instrumental analyses including FE-SEM, FTIR, and XPS. The Boehm titration method indicated the presence of multiple oxygen groups in PAC-CA6. Conclusively, the mechanism of Co(II) adsorption onto PAC-CA6 involved electrostatic interactions between Co(II) ions and carboxylic groups present on the surface of PAC-CA6. From the result, the PAC-CA6 could be sufficiently used as a potential adsorbent for the removal of cobalt from aqueous solutions.

Keywords: Petroleum Residue, Carboxylation, Co(II), Adsorption

INTRODUCTION

Cobalt (Co) exists as ^{59}Co in its stable form and as ^{56}Co, ^{57}Co, ^{58}Co, and ^{60}Co in its radioactive isotopes [1,2]. This versatile metal is used in various industries, with ^{60}Co being an important component in nuclear weapons and facilities [3,4]. However, high concentrations of Co generated from these facilities are released into both land and water systems as radioactive wastes, causing detrimental effects on the ecosystem and environment owing to its chemical toxicity and gamma-ray emission [5-7]. Additionally, Co-processing industries, such as fossil fuel production, phosphate fertilizer manufacturing, mining, Co ore smelting, and Co alloy processing, release Co into the environment [8-16]. All Co isotopes exhibit similar chemical behavior and environmental effects [17]. Long-term exposure to Co can lead to lung disease, heart problems, thyroid dysfunction, and gastrointestinal issues such as nausea, vomiting, and diarrhea [18,19]. Therefore, development of novel technologies for removing Co from the environment is pertinent.

Co can be removed from the environment using various techniques, including precipitation, ion exchange, advanced oxidation processes, membrane filtration, and adsorption [20-26]. Adsorption is an effective and reliable physicochemical method, as it is cost-efficient, involves a simple process that is easy to operate and does not generate any by-products. Therefore, many researchers have investigated inexpensive raw materials for the development of adsorbents.

During fractional distillation and refining of crude oil, petroleum residues are excessively produced along with petroleum. With the development of the petroleum industry, the amount of petroleum residues generated during oil refining has been increasing globally. These residues contain thousands of polyaromatic hydrocarbons (PAHs) [27]. Petroleum pitch, a residue obtained from the pyrolysis of organic matter or the distillation of tar, is composed of complex mixtures of several types of aromatic hydrocarbons and heterocyclic compounds [28-31]. Petroleum pitch derived from petroleum residues can be utilized as a carbon precursor owing to its high PAH content. The resulting carbon compound is environmentally friendly, chemically stable, and easily reformable with oxygen and metals. Therefore, petroleum pitch can be used to enhance the adsorption capacity of adsorbents [32-36]. Zhang et al. conducted a study on the petroleum pitch used for the removal of methylene blue and direct black dyes, and Wang et al. developed a petroleum pitch-based aromatic framework with phosphonate ligands for the removal of radioactive uranium [37,38]. However, research on the development of adsorbents using petroleum pitch derived from petroleum residues is limited. Furthermore, the ability of petroleum pitch to adsorb Co ions has not been investigated.

In this study, a carboxylic-functionalized petroleum residue-activated carbon (PAC) was developed as a novel approach for the removal of Co ions. Moreover, the effects of various factors on the removal of Co ions from the environment were investigated.

MATERIALS AND METHODS

1. Preparation of PAC through Modification of Organic Acid

There are several kinds of petroleum residue oil such as pyrolysis fuel oil (PFO), fluidized catalytic cracking-decant oil (FCC-DO),

†To whom correspondence should be addressed.
E-mail: sschoi@semyung.ac.kr

and vacuum residue (VR). Of these, PFO was used for this study. The PAC was obtained from carbonization of pitch produced in the crude oil refining process and then manufactured through a carbon dioxide gasification like char preparation [39-43]. The PAC was sieved to obtain a particle size of less than 100 μm. For the surface carboxylation of PAC, two modifying agents, formic acid (FA, 99.0%, Samchun Chemical, Korea) and citric acid (99.5%, Samchun Chemical, Korea), were used. To 100 mL of 2 M modifying agent, 2 g of PAC was added and reacted at 60 °C for 24 h. The resulting product was washed with distilled water several times and dried at 60 °C for 4 h. The modified PACs were named PAC-FA2 and PAC-CA2. After the performance of these materials for Co(II) adsorption was evaluated, the concentration of citric acid was varied (2, 4, 6, 8, and 10 M) to further modify PAC (PAC-CAn, where n is the concentration of the modified citric acid) and evaluate its adsorption capability.

2. Batch Adsorption Experiments

A stock solution of 100 mg/L Co(II) was prepared by dissolving 0.224 g of $CoCl_2 \cdot 6H_2O$ (99.0%, Sigma Aldrich, USA) in 1 L of ultrapure water. The desired concentration of Co(II) solution for subsequent experiments was prepared by diluting the Co(II) stock solution. For all batch experiments, 0.2 g of the adsorbent was transferred to 100 mL of the solution adjusted to pH 6 and agitated at 25 °C for 24 h using a floor-standing shaking incubator. The pH of the solution was titrated using HCl or NaOH (0.1 M) as required.

Initially, the Co(II) adsorption performance of the adsorbents impregnated with organic acids was evaluated by comparing PAC-FA2, PAC-CA2, and PAC. Based on this result, PAC was impregnated with selected organic acids at several concentrations (2, 4, 6, 8, and 10 M), and the Co(II) adsorption capacity of the resulting PAC was determined.

Subsequently, the Co(II) adsorption capacity of PAC-CA6, which was selected as the optimum modification based on previous experiments, in an aqueous system was investigated. The effect of pH on Co(II) adsorption capacity of PAC-CA6 under different solution pH conditions (2.0, 4.0, 5.0, 6.0, 7.0, 8.0, and 10.0) was investigated. The adsorption kinetics were evaluated by determining the effect of adsorption contact time (5, 10, 15, and 20 min) at each temperature (25, 37, and 49 °C). To a flask containing 100 mL of Co(II) solution, 0.2 g of the adsorbent was transferred, and the supernatant was collected using a syringe at predetermined time intervals for 2 h. The adsorption isotherm was determined based on the initial concentration of the Co(II) solution (5, 10, 50, 75, and 100 mg/L).

After the adsorption reaction, the solution was filtered using a membrane syringe filter with a pore size of 0.45 μm, and the initial and equilibrium concentrations of the Co(II) solution were analyzed using atomic absorption spectroscopy (AAS, AA-7000, Shimadzu, Japan). Each experiment was conducted thrice to ensure reproducibility, and the average value was used for data analysis.

The amount of Co(II) adsorbed on the adsorbent at equilibrium and removal efficiency were calculated using the following equation [44]:

$$q_e\ (\mathrm{mg/g}) = (C_0 - C_e) \times \frac{V}{m} \tag{1}$$

$$\text{Removal}\ (\%) = \frac{(C_0 - C_e)}{C_0} \times 100 \tag{2}$$

where q_e is the amount of Co(II) adsorbed per unit weight of adsorbent (mg/g), C_0 (mg/L) is the initial Co(II) concentration, C_e (mg/L) is the Co(II) concentration at equilibrium, V is the volume of the Co(II) solution (L), and m is the adsorbent mass used in the adsorption experiment (g).

3. Characterization of Modified PACs

The physicochemical characterization of the modified PACs was performed using the following method. The point of zero charges (pH_{pzc}) was confirmed to determine the adsorbent surface charge [45]. The dissolved CO_2 in the distilled water was removed using 99.9% N_2 gas purged for 30 min, and free CO_2 distilled water was used for analysis. The treated distilled water was adjusted to pH 2.0 to 10.0 by adding sodium hydroxide (NaOH, bead, 98.0%, Samchun Chemical, Korea) or hydrochloric acid solution (HCl, 37.0%, Samchun Chemical, Korea), and the pH value was referred to as $pH_{Initial}$. 150 mg of the material was added to each 50 mL of pH-adjusted distilled water and stirred at 25 °C for 24 h using a floor-standing shaking incubator (JSSI-300C, JSR, Korea). Thereafter, the suspension was filtered using a 5 μm pore filter paper (No. 2, Advantec, Japan), and the pH of the filtrate solution was measured (pH_{Final}). The pH change value ($\Delta pH = pH_{Initial} - pH_{Fianl}$) relative to the initial pH was plotted. The pH at which ΔpH=0 was denoted as pH_{pzc}.

Boehm titration is a method for quantifying the specific oxygen-containing surface functional groups of carbon materials [46,47]. 25 of a 0.05 M solution of Boehm's reactants as NaOH (98.0%), Na_2CO_3 (99.0%), $NaHCO_3$ (99.0%), and HCl (36.0%) (Samchun Chemical, Korea) was equilibrated with 0.1 g of the material at 25 °C for 24 h. At the same time, a blank sample containing no material was also prepared. Then, the material was filtered from the solution, and the amount of neutralization of the separated solution was determined using a 0.1 M NaOH and HCl solution. The basic principle of titration is that strong acids and strong bases react with all bases and acids, respectively, whereas weak acids donate protons only to the conjugate bases of acids with higher pK_a values. In this way, the basic sites were counted the amount HCl reacting with surface functional groups of the adsorbent. The various free acidic groups were as follows: (i) NaOH (pK_a: 15.7) neutralized the carboxyl, lactone, and phenolic groups; (ii) Na_2CO_3 (pK_a: 10.3) neutralized the carboxyl and lactone groups; and (iii) $NaHCO_3$ (pK_a: 6.4) neutralized the carboxyl groups. Then, the excess base or acid was measured by back titration using 0.10 M NaOH and HCl solutions to determine the number of each functional group.

The porous structure and surface morphology of the materials were observed using JSM a 7100F model of field emission-scanning electron microscope (FE-SEM, JEOL, Japan). X-ray spectroscopy (EDS) chemical elemental mapping images were obtained using energy-dispersive EDS interconnected with a FE-SEM. Specific surface area was determined using the Brunauer, Emmett, and Teller (BET) method with the ASAP 2420 analyzer (Micromeritics, USA). The Fourier-transform infrared (FTIR) spectra of the materials were analyzed from the IR Tracer-100 model of FTIR spectrometer (Shimadzu, Japan). IR transmittance data were acquired for wave-

numbers of 500-4,000 cm^{-1}. The surface complexes of the sample were analyzed using X-ray photoelectron spectroscopy (XPS) using an instrument (K-alpha+, Thermo Scientific, United States) equipped with a monochromatized Al Kα radiation source.

4. Theoretical Models

Adsorption equilibrium is important for predicting pollutant adsorption behavior on the adsorbent surface during adsorption processes. The equilibrium data obtained from the Co(II) batch adsorption experiments on PAC and PAC-CA6 were analyzed using the Freundlich, Langmuir, and Temkin adsorption isotherm models.

The Freundlich isotherm describes the multilayer formation of an adsorbate on an adsorbent [48]. The linearized form is expressed as follows:

$$\ln q_e = \ln k_F + \frac{1}{n}\ln C_e \tag{3}$$

where k_F (mg/g) is the Freundlich constant and n is the adsorption strength. A linear plot of $\log q_e$ vs. $\log C_e$ was used to calculate the Freundlich constant.

The Langmuir adsorption isotherm model describes monolayer complexation of the adsorbate on the adsorbent [49]. The linear equation can be determined as follows:

$$\frac{C_e}{q_e} = \frac{C_e}{q_{max}} + \frac{1}{q_{max}\cdot k_L} \tag{4}$$

where C_e is the concentration of Co(II) at the equilibrium solution (mg/L), and q_e is the Co(II) adsorption capacity (mg/g). q_{max} (mg/g) is the maximum Co(II) adsorption capacity of the adsorbent and k_L (L/mg) is the Langmuir constant related to the adsorption energy. A linear plot of C_e versus C_e/q_e was used to calculate the Langmuir constants. Based on the Langmuir equation, the separation factor (R_L) and the surface coverage (θ) are derived as follows. The separation factor indicates the preference for adsorption [50].

$$R_L = \frac{1}{1+k_L\cdot C_0} \tag{5}$$

where C_0 is the various initial concentrations of the Co(II) in the adsorption isotherm experiments. The R_L value indicates whether the isotherm is favorable ($0<R_L<1$) or unfavorable ($R_L>1$). Surface coverage (θ) can help to understand the nature of the adsorption process [51]. The equation used is as follows:

$$\theta = \frac{k_L\cdot C_0}{1+k_L\cdot C_0} \tag{6}$$

where k_L is the Langmuir constant and C_0 is the initial Co(II) concentration.

The Temkin isotherm model is based on the indirect interaction of the adsorbate with the adsorbate [52].

$$q_e = \frac{R\cdot T}{b_T}\cdot \ln k_T + \frac{R\cdot T}{b_T}\cdot \ln C_e \tag{7}$$

where b_T is the Temkin constant related to the adsorption heat (J/mol), and k_T (L/mg) is the Temkin binding constant. R is the ideal gas constant (8.314 J/mol·K), and T is temperature (K).

Adsorption kinetic studies are important for adsorption processes because they describe the absorption rate of the adsorbate and control the residence time of the entire adsorption process. Therefore, in this study, Co(II) removal kinetics was investigated to understand the behavior of the adsorbent. Three kinetic models were used to describe the adsorption process: pseudo-first-order (PFO), pseudo-second-order (PSO), and Elovich.

PFO was calculated as if it were a first-order reaction, although it was originally a second-order reaction when the concentration of one of the two reactants was relatively high [53]. The PFO model is expressed as follows:

$$\ln(q_e - q_t) = \ln q_e - k_1\cdot t \tag{8}$$

where q_t and q_e (mg/g) are the adsorption capacities at time and equilibrium time, respectively. k_1 (1/min) is the kinetic rate constant of PFO. The value of k_1 can be obtained from plotting $\ln(q_e-q_t)$ against t for the experimental results.

PSO assumes that the adsorption reaction depends on the adsorbate and the concentration of the adsorbent, which is usually the case in the rate-limiting step [54]. The PSO model is expressed as follows:

$$\frac{t}{q_t} = \frac{t}{q_e} + \frac{1}{k_2\cdot q_e^2} \tag{9}$$

where k_2 (g/mg·min) is the kinetic rate constant of the PSO. The value of k_2 was determined by plotting t/q_t against t and obtaining the slope of the resulting line.

The Elovich model helps predict the mass, surface diffusion, and activation energies of a system [55]. It is utilized to better understand the chemisorption properties of adsorption, and it assumes that the adsorption rate of the solute decreases drastically as the amount of solute adsorbed increases [56]. The Elovich model is expressed as follows:

$$q_t = \beta\ln(\alpha\cdot\beta) + \beta\ln t \tag{10}$$

where, α is the initial adsorption rate (mg/(g·min)), and β is the desorption constant (g/mg). The value of α and β were calculated from the linear plot of the slope and intercept the adsorption data using q_t vs ln t.

RESULTS AND DISCUSSION

1. Evaluation of Adsorption Capacity

This experiment aimed to determine the optimal modified organic acid concentration for removing Co(II) from water using PAC modified with formic acid and citric acids. Fig. 1(a) shows that PAC-CA2 modified with citric acid had a higher Co(II) adsorption capacity (8.16 mg/g) than that of PAC-FA2 modified with formic acid (6.79 mg/g). The Co(II) adsorption efficiency of PAC-CA2 was 2.23 times higher than that of raw PAC. The higher Co(II) adsorption capacity of PAC-CA2 can be explained by the presence of many carboxylic groups in citric acid.

As shown in Fig. 1(b), the Co(II) adsorption capacity of the PACs modified with various concentrations of citric acid was evaluated. As the concentration of the citric acid solution increased to 6 M, the adsorption capacity of Co(II) also increased. However, PAC-CA8 and PAC-CA10 showed a gradual decrease in Co(II)

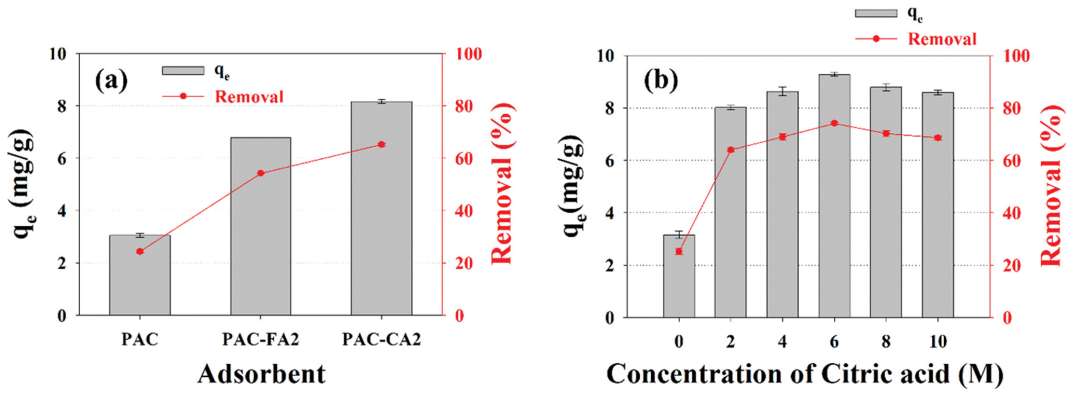

Fig. 1. Co(II) adsorption capacity using different organic acid (a), Co(II) adsorption capacity using modified PAC by different concentrations of citric acid (b).

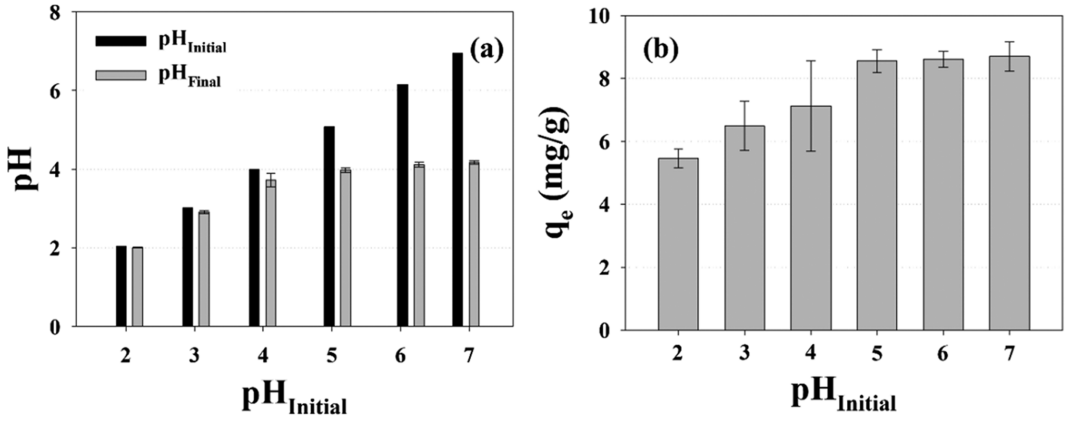

Fig. 2. pH_{intial} and pH_{Final} after transferring PAC-CA6 to Co(II) solution at each pH (a), Effect of pH on the adsorption of Co(II) using PAC-CA6 (b) (Initial Co(II): 25 mg/L, PAC-CA6 dose: 2.0 g/L, reaction time: 24 h, reaction temperature: 25 °C, stirring speed: 150 rpm).

adsorption behavior. It was concluded that the sites capable of adsorbing Co(II) were buried by citric acid when the concentration of the modified citric acid solution was higher than 6 M. From these results, PAC-CA6 modified with 6 M citric acid was selected as the optimal modification condition.

The effects of the initial pH of the Co(II) solution on the pH before and after the transfer of PAC-CA6 (Fig. 2(a)) and the adsorption capacity of Co(II) (Fig. 2(b)) were also investigated. When the pH exceeded 8, the precipitation of Co(II) began. Therefore, the experimental $pH_{Initial}$ conditions were controlled between 2 and 7. As the $pH_{Initial}$ of the solution increased, the range of change in pH increased, and as $pH_{Initial}$ increased, pH_{Final} tended to equilibrate to approximately 4. This appeared to decrease the pH of the solution by the surface charge pH_{pzc} of PAC-CA6. More specifically, the proton of the carboxylic group present on the surface of PAC-CA6 dissociated into the solution to acidify the liquid phase of the solution. The results show that the optimal adsorption efficiency was achieved between pH 5 and 7, and as the initial pH of the solution increased, the amount of Co(II) adsorbed increased. The pH_{Final} of this section was like each other at 4, and it is expected that the speciation of citric acid of PAC-CA6 is similar, and because of this, the adsorption amount of Co(II) is judged to be similar.

Isothermal adsorption was performed using a wide range of Co(II) concentration (5-100 mg/L) to investigate the effect of the initial concentration on the adsorption of PAC-CA6 (Fig. 3(a)). The isothermal adsorption results were applied to Freundlich, Langmuir, and Temkin adsorption isotherms, which are widely used to derive adsorption mechanisms and parameters, and the resulting isothermal adsorption parameters are shown in Table 1. Comparing the correlation coefficients r^2 of the three models, Langmuir> Temkin>Freundlich was found to be suitable in the order. The

Table 1. Adsorption isotherms parameters for Co(II) adsorption using PAC-CA6

Models	Parameters	PAC-CA6
Freundlich	k_F (mg/g)	1.626
	n	2.731
	r^2	0.866
Langmuir	k_L (L/mg)	0.309
	q_{max} (mg/g)	12.500
	r^2	0.999
Temkin	k_T (L/mg)	4.572
	b_T (kJ/mol)	1.119
	r^2	0.950

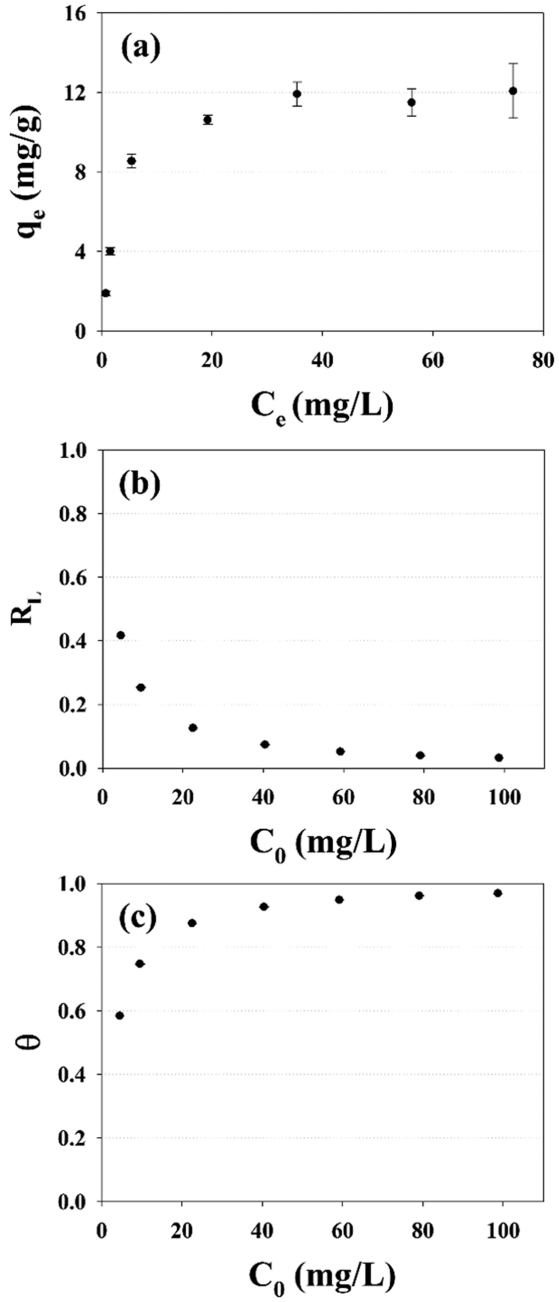

Fig. 3. Effect of initial concentration of Co(II) on adsorption capacity (PAC-CA6 dose: 2.0 g/L, pH 6, reaction time: 24 h, reaction temperature: 25 °C, stirring speed: 150 rpm).

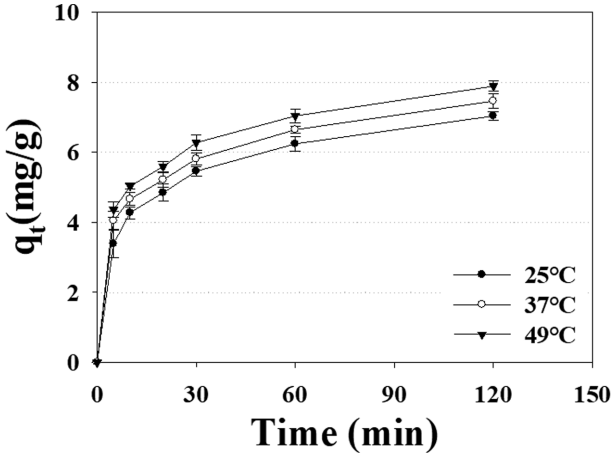

Fig. 4. Effect of the reaction time for the removal of Co(II) using PAC-CA6 on each temperature (Initial Co(II): 25 mg/L, PAC-CA6 dose: 2.0 g/L, pH 6, reaction temperature: 25, 37, 49 °C, stirring speed: 150 rpm).

maximum adsorption capacity (q_{max}) of Co(II) for PAC-CA6 was calculated as the 12.50 mg/g using Langmuir isotherm. These values were compared with those of other materials tested for Co(II) adsorption capacity (Table 2) [57-62]. Although not based on a comprehensive investigation, it was shown that PAC-CA6 has a greater Co(II) adsorption capacity than many previously studied materials. According to the Temkin isotherm, the thermal energy k_T released during adsorption was 1.119 kJ/mol. The suitability of the adsorption process of PAC-CA6 was calculated as the separation factor, R_L, at various initial concentrations based on the Langmuir isotherm and is presented in Fig. 3(b). The R_L values ranging from 0 to 1 indicate that PAC-CA6 is favorable for Co(II) adsorption [63]. The adsorption characteristics of Co(II) on PAC-CA6 can be understood in more detail as the surface coverage, θ, and θ for the initial concentration of Co(II) are shown in Fig. 3(c). At first, θ increased rapidly as the initial concentration increased, but as the concentration of Co(II) exceeded 40 mg/L, the θ value approached 1 and the increase decreased. This implies that the surface of PAC-CA6 is densely covered with a Co(II) monolayer [51]. The Langmuir model fitted the adsorption isotherm data, indicating that the adsorption of Co(II) by PAC-CA6 follows a monolayer adsorption mechanism. The separation coefficient and surface coverage obtained from the Langmuir isotherm parameters suggest that PAC-CA6 has high affinity and capacity for Co(II) adsorption.

Table 2. Comparison of adsorption capacities for Co(II) by various adsorbents

Adsorbents	q_{max} (mg/g)	Condition	Reference
Saccharomyces cerevisiae cells	0.68	pH 8, 25 °C	[57]
Palygorskite	8.88	pH 7.8, 35 °C	[58]
spent coffee	5.37	pH 5.8, 20 °C	[59]
Anaerobic granular sludges	8.92	pH 7, 30 °C	[60]
Kaolinite	1.470	40 °C	[61]
Chitosan-g-maleic acid	2.78	26 °C	[62]
PAC-CA6	12.50	pH 6, 20 °C	This work

Table 3. Adsorption kinetics parameters for the Co(II) adsorption using PAC-CA6

Models	Parameters	25 °C	37 °C	49 °C
PFO	q_e (mg/g)	7.219	7.628	8.036
	k_1 (1/min)	0.027	0.038	0.029
	r^2	0.985	0.971	0.989
PSO	q_e (mg/g)	7.457	7.849	8.271
	k_2 (g/(mg·min))	0.022	0.017	0.014
	r^2	0.997	0.994	0.997
Elovich	α (mg/g·min))	3.441	6.775	7.972
	β (g/mg)	1.141	1.086	1.119
	r^2	0.997	0.991	0.993

The Co(II) adsorption of PAC-CA6 as a function of temperature and time is shown in Fig. 4, and the adsorption kinetic parameters are summarized in Table 3. The mechanisms of the adsorption kinetics of the PFO, PSO, and Elovich models were evaluated using experimental data obtained from the effect on adsorption during the reaction time (120 min). PAC-CA6 and Co(II) showed fast adsorption rates, regardless of the temperature, in the primary step of the reaction, and the rate gradually decreased. Rapid adsorption in the initial stage occurred because there were sufficient usable adsorption sites for PAC-CA6 and Co(II) to be properly adsorbed. As the reaction continues, the sites where Co(II) can adsorb become saturated, and the reaction rate decreases. By comparing the correlation coefficients of the adsorption kinetics model of PAC-CA6, PSO>Elovich>PFO was found to be suitable in the order. The PSO model fit indicated that the adsorption rate depended on the adsorption capacity rather than the adsorbate concentration, and this behavior was predicted over the entire adsorption range based on the assumption that chemisorption was the limiting step [64,65]. The Elovich model fit indicated that chemisorption on the surface of PAC-CA6 was energetically heterogeneous. The study also found that as the temperature increased, the adsorption rate constant (k_2) decreased, while the adsorption rate (α) increased. Additionally, this study suggests that PAC-CA6 has a highly nega-

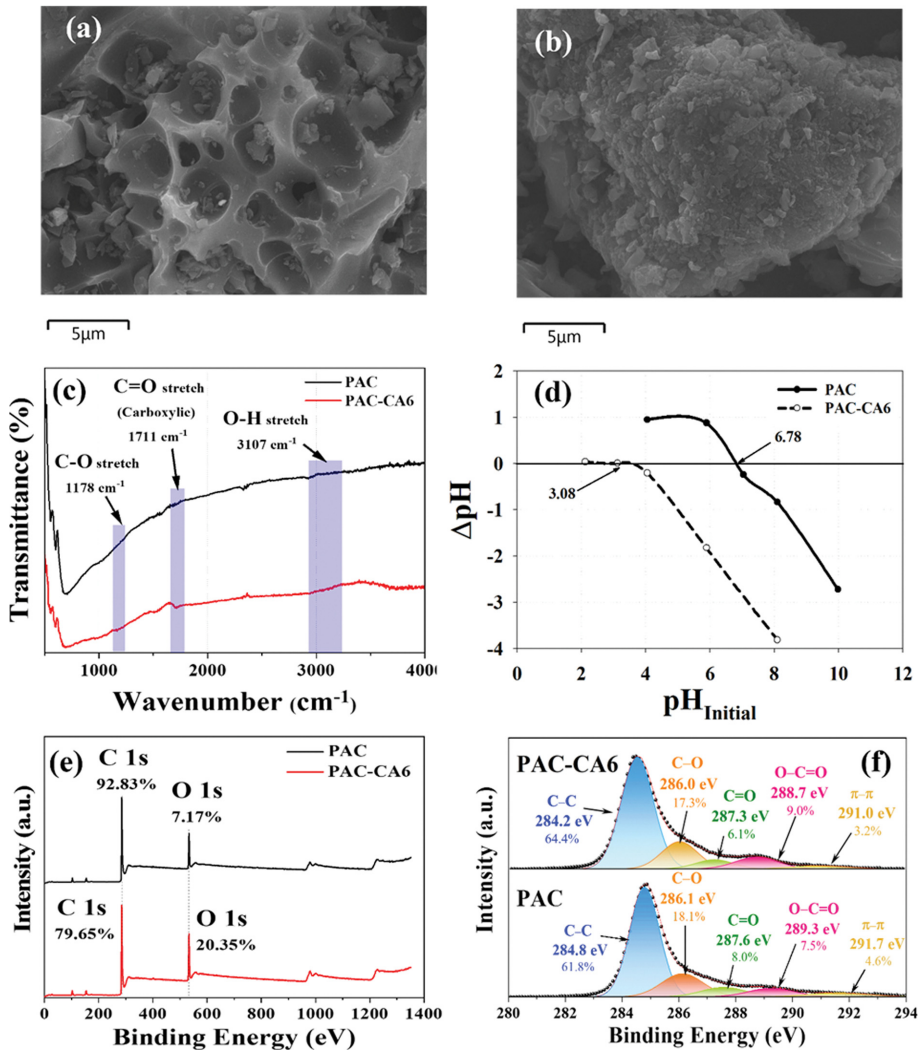

Fig. 5. FE-SEM images of PAC (a) and PAC-CA6 (b), FTIR spectra (c), pH_{pzc} (d), XPS survey spectrum with C 1s and O 1s atomic weight ratio (e), fitting curves of C 1s for PAC and PAC-CA6 (f).

tively charged surface, which reduces the time required to reach the adsorption equilibrium.

2. Characterization of Adsorbents

Fig. 5 shows FE-SEM images of PAC and PAC-CA6. As shown in Fig. 5(a), PAC appears as a porous material with irregularly sized pores and contains impurities such as residual oil waste on its surface. In contrast, PAC-CA6 modified with citric acid showed crystallization and attachment of citric acid on its surface (Fig. 5(b)). This modification introduces functional groups that enhance the ion exchange capacity of the adsorbent during the adsorption process. The specific surface area of PAC decreased from 286.50 m^2/g to 34.18 m^2/g because of filling or blocking the pores due to the modification of citric acid on the surface of PAC, as shown in the SEM. The FTIR spectra of PAC and PAC-CA6 in Fig. 5(c) confirm the presence of carboxylic and other functional groups resulting from the attachment of citric acid. Specifically, peaks related to citric acid, such as C-O (1,178 cm^{-1}), C=O (1,711 cm^{-1}), and O-H (3,107 cm^{-1}), were observed on the surface of PAC-CA6 but not on PAC. These additional peaks suggest the presence of citric acid [66]. Overall, the functional groups on the surface of PAC-CA6 play a crucial role in increasing the Co(II) adsorption capacity during the adsorption process. Table 4 shows the estimated oxygen functional groups of PAC and PAC-CA6 obtained from the Boehm titration measurements. The results indicate that the overall oxygen functional groups, including the carboxylic group, increased after citric acid modification on the surface of PAC. This increase was confirmed by the measurements. Fig. 5(d) shows the ΔpH of the solution by PAC and PAC-CA6. The pH_{pzc} is the chemical and electrical potentials of the adsorbent particle surface and was found to be 6.78 and 3.08 for PAC and PAC-CA6, respectively. Notably, the pH_{pzc} value of the PAC decreased after modification with citric acid. This decrease is attributed to the oxygen functional group, specifically the carboxylic group, introduced by the citric acid modification. This characteristic was expected to enhance the ability of PAC-CA6 to exchange anions with Co(II) during adsorption [67, 68]. XPS analysis was also performed on both PAC and PAC-CA6 to confirm the fraction of each element and to investigate the bonding structure of carbon (Fig. 5(e) and (f)). The results show that the C/O ratios of PAC and PAC-CA6 were 12.9 and 3.9, respectively. PAC had a higher C/O ratio because it served as a carbon precursor, whereas PAC-CA6 had a reduced C/O ratio owing to the incorporation of oxygen through bonding with citric acid. Bond structure analysis revealed that the fractions of C-C and O-C=O bonds in PAC increased after modification with citric acid, whereas the fractions of C-O and C=O bonds decreased. It was speculated that the C-O and C=O bonds on the PAC surface formed substitution bonds with the carboxylic group of citric acid, leading to a decrease in their fraction and an increase in the carboxylic groups.

Table 4. Boehm titration results of PAC and PAC-CA6

Adsorbents	Phenolic (mmol/g)	Lactonic (mmol/g)	Carboxylic (mmol/g)	Total acidity (mmol/g)
PAC	0.363	0.215	0.373	0.951
PAC-CA6	0.512	0.340	1.866	2.717

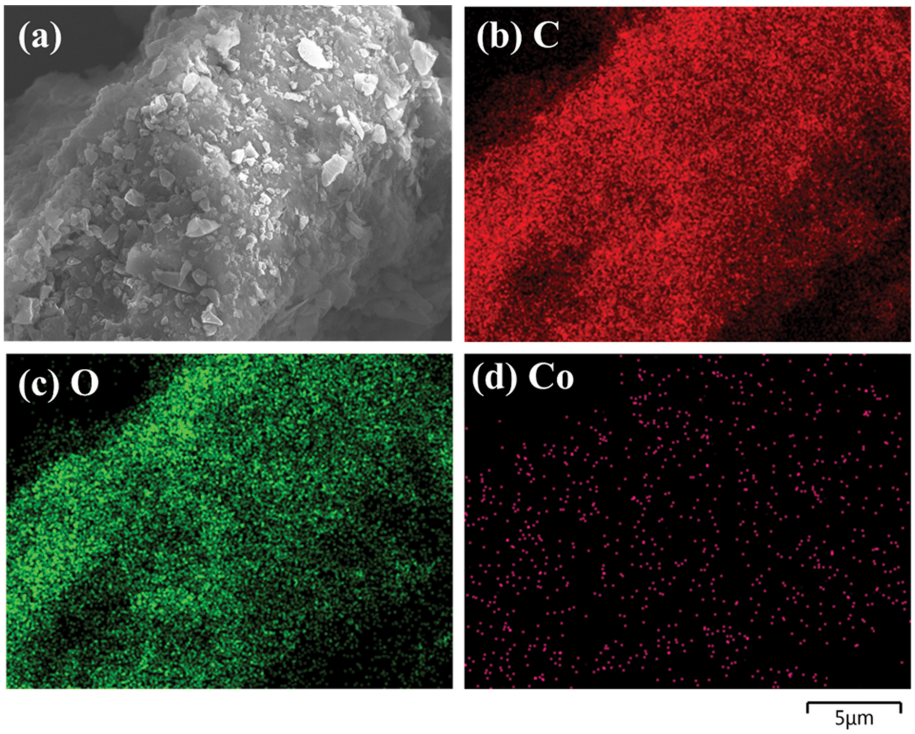

Fig. 6. Element mapping of Co(II) adsorbed using PAC-CA6.

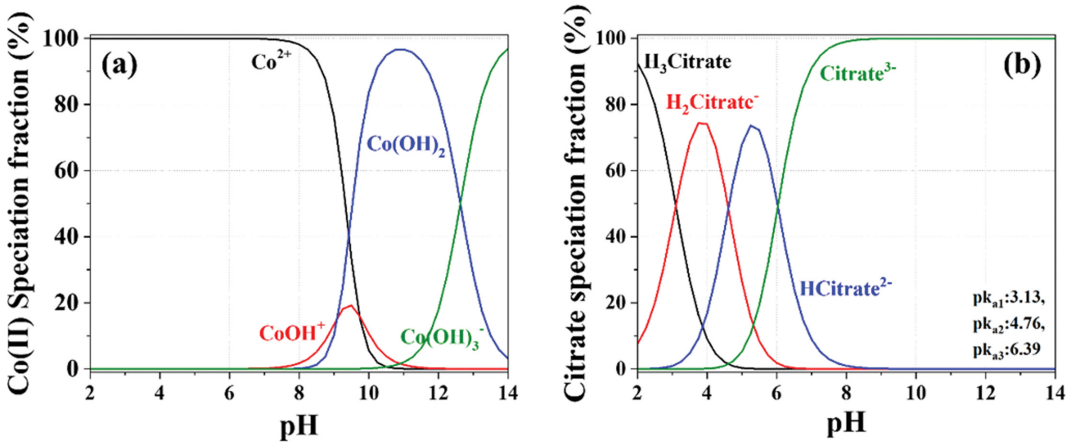

Fig. 7. Speciation diagram for Co(II) (a) and citrate (b) in an aqueous system.

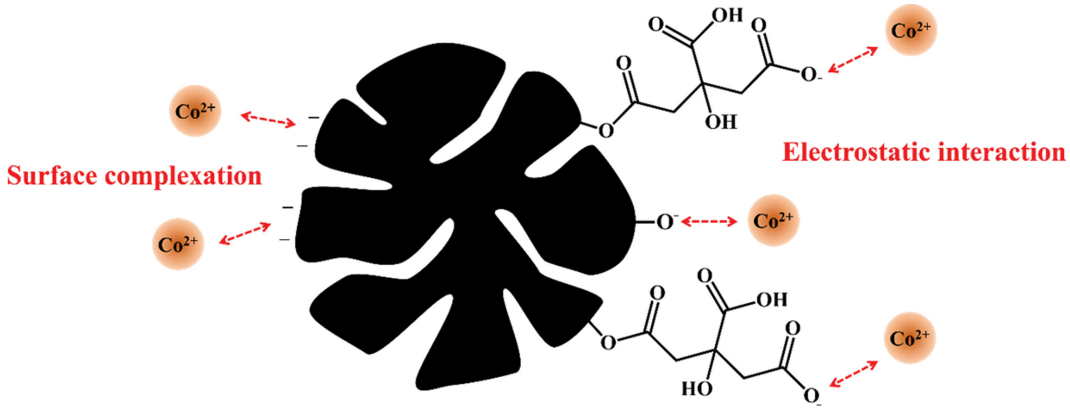

Fig. 8. Scheme of Co(II) adsorption mechanism on the PAC-CA6.

The physicochemical analysis of PAC-CA6 revealed the existence of a significant number of carboxylic groups on the surface of PAC that can form bonds with Co(II).

An EDS elements mapping images of the PAC-CA6 surface was observed after Co(II) adsorption (Fig. 6). After adsorption, the structure of citric acid bonded to the surface was stable, and it was confirmed that Co(II) was bonded to the center of the C and O structure formed by citric acid bonding. The speciation fractions of Co(II) (a) and Citric acid (b) each pH are presented on Fig. 7. In the case of Co(II), as the pH increases above 7, it is gradually converted into chemical species ($CoOH^+$, $Co(OH)_2$, and $Co(OH)_3^-$) combined with OH groups and precipitates [69]. As the pH increased, the pk_a values of citric acid were 3.13, 4.76, and 6.39, and the protons of the carboxylic group were lost and became negatively charged [70]. Because the citric acid present in PAC-CA6 exists in a bonded state to the surface of PAC, the pk_a value of citric acid does not follow the expectation; however, as the pH increases, Co(II) adsorb to each other as the pH decreases. A favorable environment will be created.

3. Adsorption Mechanism

The expected mechanism of Co(II) adsorption on PAC-CA6 is shown in Fig. 8. Based on the characterization and adsorption experiments, it was determined that the mechanism of Co(II) adsorption onto PAC-CA6 involved the formation of a carboxylic group through substitution with an oxygen functional group on the surface of the PAC. This is a functional group formed by citric acid modification that partially follows the characteristics of citric acid. This carboxylic group partially follows the characteristics of citric acid, with pk_a values (3.13, 4.76, and 6.39), which allows it to become negatively charged at higher pH levels, which is beneficial for combination with Co(II), as confirmed through pH effect experiments (Fig. 2(b)). In addition, isothermal adsorption and kinetic experiments revealed that rate-limiting and chemical adsorption were achieved in the monolayer form. Therefore, it was found that Co(II) and the carboxylic group formed in PAC-CA6 formed a strong electrostatic interaction by covalent bonding with opposite charges.

CONCLUSIONS

This study investigated the physicochemical properties of carboxylate carbon-based PAC, as well as its efficacy in adsorbing and removing Co(II) from water phase. Physicochemical characterization of PAC-CA6, such as FE–SEM, FTIR, pH_{pzc}, and XPS, confirmed that oxygen functional groups were formed on the surface of the PAC. Boehm titration analysis further suggests the presence of oxygen functional groups that facilitate Co(II) bonding on the

surface. The maximum Co(II) adsorption capacity of PAC-CA6 was found to be 12.50 mg/g, and the Langmuir isotherm was deemed the best fit compared with the Freundlich and Temkin isotherms. The calculated R_L and θ were between 0 and 1.0, confirming that the adsorption process for Co(II) was suitable for PAC-CA6. In addition, the adsorption mechanism of Co using PAC-CA6 can be explained by chemical adsorption based on the results of the PSO and Elovich model. The experimental results indicated that PAC-CA6 has great potential as an ideal adsorbent for Co(II) removal from aqueous systems.

ACKNOWLEDGEMENTS

This work was supported by the Industrial Strategic Technology Development Program (20012763, development of petroleum residue-based porous adsorbent for industrial wastewater) funded by the Ministry of Trade, Industry, and Energy (MOTIE, Korea).

REFERENCES

1. M. Dawoud, M. Hegazy, W. Helew and H. Saleh, *J. Nucl. Energy Sci. Power Gener. Technol.*, **3**, 10 (2021).
2. J. Livingood and G. Seaborg, *Phys. Rev.*, **60**, 913 (1941).
3. M. C. Lagunas-Solar, *J. Food Prot.*, **58**, 186 (1995).
4. M. H. Pham, C. Yu, M. Rusch, C. Holloway, E. Chang and M. L. Apuzzo, *World Neurosurg.*, **82**, 1060 (2014).
5. A. Abdelnour-Esquivel, J. Perez, M. Rojas, W. Vargas and A. Gatica-Arias, *In Vitro Cell. Dev. Biol. Plant*, **56**, 88 (2020).
6. R. . Gephart, *Phys. Chem. Earth.*, **35**, 298 (2010).
7. L. G. Yamamoto, *Pediatr. Emerg. Care*, **29**, 1016 (2013).
8. D.-M. Bordean, A.-B. Borozan, D. Nica, S. Alda, L. Cojocaru, M. Horablaga, N. Filimon and I. Gergen, *Int. Multidiscip. Sci. GeoConference Surv. Geol. Min. Ecol. Manag. SGEM*, **5**, 101 (2012).
9. A. B. Botelho Junior, D. B. Dreisinger and D. C. Espinosa, *Min. Metall. Explor.*, **36**, 199 (2019).
10. U.-K. Hwang, H.-M. Ryu, Y.-H. Choi, S.-M. Lee and H.-S. Kang, *Korean J. Environ. Biol.*, **29**, 251 (2011).
11. S. Jahan and V. Strezov, *PloS One*, **12**, 0189284 (2017).
12. M. Jiang, K. Wang, Y. Wang, Q. Zhao and W. Wang, *Sci. Total Environ.*, **813**, 151908 (2021).
13. J. Kettelarij, K. Midander, C. Lidén and A. Julander, *Contact Derm.*, **79**, 226 (2018).
14. M. J. Lain, *J. Power Sources*, **97**, 736 (2001).
15. L. Li, J. Lu, Y. Ren, X. X. Zhang, R. J. Chen, F. Wu and K. Amine, *J. Power Sources*, **218**, 21 (2012).
16. E. M. Melchor-Martínez, R. Macias-Garbett, A. Malacara-Becerra, H. M. Iqbal, J. E. Sosa-Hernández and R. Parra-Saldívar, *Case Stud. Chem. Environ. Eng.*, **3**, 100104 (2021).
17. S. Tao, T. Wang, Y. Wu, C. Wang and G. Wang, *J. Hazard. Mater.*, **415**, 125680 (2021).
18. L. Leyssens, B. Vinck, C. Van Der Straeten, F. Wuyts and L. Maes, *Toxicology*, **387**, 43 (2017).
19. S. Mahey, R. Kumar, M. Sharma, V. Kumar and R. Bhardwaj, *SN Appl. Sci.*, **2**, 665 (2020).
20. A. Bhatnagar, A. Minocha and M. Sillanpää, *Biochem. Eng. J.*, **48**, 181 (2010).
21. A. B. Botelho Junior, D. B. Dreisinger and D. C. Espinosa, *Mining, Metallurgy & Exploration*, **36**, 199 (2019).
22. J. Hou, X. He, S. Zhang, J. Yu, M. Feng and X. Li, *Sci. Total Environ.*, **770**, 145311 (2021).
23. M. A. Islam, D. W. Morton, B. B. Johnson, B. K. Pramanik, B. Mainali and M. J. Angove, *Environ. Nanotechnol. Monit. Manag.*, **10**, 435 (2018).
24. F. Jia, Y. Yin and J. Wang, *Prog. Nucl. Energy*, **103**, 20 (2018).
25. S. Matagi, D. Swai and R. Mugabe, *Afr. J. Trop. Hydrobiol. Fish.*, **8**, 23 (1998).
26. D. Rana, T. Matsuura, M. Kassim and A. Ismail, *Desalination*, **321**, 77 (2013).
27. W. Zhang, J. T. Andersson, H. J. Räder and K. Müllen, *Carbon*, **95**, 672 (2015).
28. G. P. Blümer, G. Collin and H. Höke, *Ind. Carbon and Graphite Mater.*, **1**, 172 (2021).
29. J. G. Kim, J. H. Kim, B.-J. Song, Y. P. Jeon, C. W. Lee, Y.-S. Lee and J. S. Im, *Fuel*, **167**, 25 (2016).
30. A. Martínez-Alonso, J. Bermejo and J. Tascón, *J. Therm. Anal.*, **38**, 811 (1992).
31. M. Pérez, M. Granda, R. Santamaría, T. Morgan and R. Menéndez, *Fuel*, **83**, 1257 (2004).
32. C. H. Kwak, C. Lim, S. Kim and Y.-S. Lee, *J. Ind. Eng. Chem.*, **116**, 21 (2022).
33. Q. Gao, L. Demarconnay, E. Raymundo-Piñero and F. Béguin, *Energy Environ. Sci.*, **5**, 9611 (2012).
34. C. W. Tan, K. H. Tan, Y. T. Ong, A. R. Mohamed, S. H. S. Zein and S. H. Tan, *Environ. Chem. Lett.*, **10**, 265 (2012).
35. M. Uchimiya, S. Chang and K. T. Klasson, *J. Hazard. Mater.*, **190**, 432 (2011).
36. X. Yang, Y. Wan, Y. Zheng, F. He, Z. Yu, J. Huang, H. Wang, Y. S. Ok, Y. Jiang and B. Gao, *Chem. Eng. J.*, **366**, 608 (2019).
37. T. Wang, M. Xu, X. Han, S. Yang and D. Hua, *J. Hazard. Mater.*, **368**, 214 (2019).
38. C. Zhang, Y. Li, Y. Li, W. Zhang, X. Wang, X. He and M. Yu, *Chemosphere*, **216**, 379 (2019).
39. J.-Y. Kim, S. Oh and Y.-K. Park, *J. Hazard. Mater.*, **384**, 121356 (2020).
40. X. N. Law, W. Y. Cheah, K. W. Chew, M. F. Ibrahim, Y.-K. Park, S.-H. Ho and P. L. Show, *Environ. Res.*, **204**, 111966 (2022).
41. D. Lee, H. Nam, M. W. Seo, S. H. Lee, D. Tokmurzin, S. Wang and Y.-K. Park, *Chem. Eng. J.*, **447**, 137501 (2022).
42. J. Y. Seo, D. Tokmurzin, D. Lee, S. H. Lee, M. W. Seo and Y.-K. Park, *Bioresour. Technol.*, **447**, 127740 (2022).
43. M. W. Seo, S. H. Lee, H. Nam, D. Lee, D. Tokmurzin, S. Wang and Y.-K. Park, *Bioresour. Technol.*, **343**, 126109 (2022).
44. J. R. Koduru, L. P. Lingamdinne, J. Singh and K.-H. Choo, *Process Saf. Environ. Prot.*, **103**, 87 (2016).
45. Y. Yang, Y. Chun, G. Sheng and M. Huang, *Langmuir*, **20**, 6736 (2004).
46. H. Boehm, *Carbon*, **32**, 759 (1994).
47. H. P. Boehm, *Carbon*, **40**, 145 (2002).
48. A. Proctor and J. Toro-Vazquez, *J. Am. Oil Chem. Soc.*, **73**, 1627 (1996).
49. I. Langmuir, *J. Am. Chem. Soc.*, **38**, 2221 (1916).
50. H. Lalhruaitluanga, K. Jayaram, M. Prasad and K. Kumar, *J. Haz-*

ard. Mater., **175**, 311 (2010).
51. S. Khandaker, T. Kuba, S. Kamida and Y. Uchikawa, *J. Environ. Chem. Eng.*, **5**, 1456 (2017).
52. R. D. Johnson and F. H. Arnold, *Biochim. Biophys. Acta*, **1247**, 293 (1995).
53. S. Lagergren, *Kongl. Vetensk. Acad. Handl.*, **24**, 1 (1898).
54. Y.-S. Ho and G. McKay, *Chem. Eng. J.*, **70**, 115 (1998).
55. S. Roginsky and Y. B. Zeldovich, *Acta Phys. Chem. USSR*, **1**, 2019 (1934).
56. I. McLintock, *Nature*, **216**, 1204 (1967).
57. M. Galedar and H. Younesi, *Am. J. Biochem. Biotechnol.*, **9**, 47 (2013).
58. M. He, Y. Zhu, Y. Yang, B. Han and Y. Zhang, *Appl. Clay Sci.*, **54**, 292 (2011).
59. D. Imessaoudene, S. Hanini, A. Bouzidi and A. Ararem, *Desalin. Water Treat.*, **57**, 6116 (2016).
60. E. D. van Hullebusch, M. H. Zandvoort and P. N. Lens, *J. Chem. Technol. Biotechnol.*, **79**, 1219 (2004).
61. Ö. Yavuz, Y. Altunkaynak and F. Güzel, *Water Res.*, **37**, 948 (2003).
62. S. Zhuang, Y. Yin and J. Wang, *Nucl. Eng. Technol.*, **50**, 211 (2018).
63. S. Chegrouche, A. Mellah and M. Barkat, *Desalination*, **235**, 306 (2009).
64. X. Guo and J. Wang, *J. Mol. Liq.*, **288**, 111100 (2019).
65. J. O. Ighalo, K. O. Iwuozor, C. A. Igwegbe and A. G. Adeniyi, *Colloids Surf. A: Physicochem. Eng. Asp.*, **626**, 127119 (2021).
66. M. Castro-Cabado, F. J. Parra-Ruiz, A. Casado and J. S. Roman, *Polym. Polym. Compos.*, **24**, 643 (2016).
67. M. Thirumavalavan, Y.-L. Lai and J.-F. Lee, *J. Chem. Eng. Data*, **56**, 2249 (2011).
68. L. Xia, Y. Lu, H. Meng and C. Li, *J. Hazard. Mater.*, **393**, 122487 (2020).
69. Y. Aşçı and Ş. Kaya, *Desalin. Water Treat.*, **57**, 13091 (2016).
70. A. Valverde, G. I. Tovar, N. A. Rio-López, D. Torres, M. Rosales, S. Wuttke, A. Fidalgo-Marijuan, J. M. a. Porro, M. Jiménez-Ruiz and V. García Sakai, *Chem. Mater.*, **34**, 9666 (2022).